ATMOSPHERIC CONVECTIVE STRUCTURE AND A CONVECTION SCHEME BASED ON SATURATION POINT ADJUSTMENT

A.K. Betts
West Pawlet, Vermont 05775

1. INTRODUCTION

Betts (1982a) introduced the saturation point (SP) approach to the thermodynamics of atmospheric convection and used it to discuss convective mixing processes, atmospheric convective equilibrium and instabilities, and presented examples for different convective atmospheres. Betts (1982b) proposed simple cloud thermodynamic models in SP coordinates and explored the change in cloud parcel SP associated with mixing, and both the fallout of precipitation from updrafts and its evaporation in unsaturated downdrafts. Betts (1983a) introduced SP budget diagrams in a vector notation to describe mixed stratocumulus layers as a prototype for the undisturbed boundary layer, and explored the coupling of convective mixing with the radiative flux divergence. Betts (1983b) analyzed a severe storm boundary layer to illustrate the use of SP methods to compact different data sets, formulate boundary layer budgets and understand the coupling of mixing and evaporative processes in the boundary layer outflow from cumulonimbus. The reader is referred to the papers for details. Here we shall use extracts from these papers and unpublished examples to illustrate atmospheric convective structure and then propose a convection scheme based on SP adjustment.

The underlying philosophy of this work is that it is advantageous to develop an integrated framework for the observational description and parametric modelling of atmospheric convection so that a closer interaction is facilitated. The present gulf between say, moist adiabatic adjustment and what we know about convective thermodynamic structure from observational programs needs to be bridged. I believe that useful progress can be made in this direction using SP thermodynamics as a common framework. Adjusting a numerical model toward an (observationally determined) SP structure could form the basis of a cumulus parameterization, which would have the advantage of always approaching a realistic vertical temperature and moisture structure. Several levels of complexity are possible (eg. including SP cloud parametric models (Betts, 1982b), specification of subgrid scale variances using conserved parameters, subgrid cloud distributions in terms of saturation level so as to model radiative fluxes with greater realism, time evolving cloud fields).

In this paper we shall just introduce the simplest concept, which could be regarded as a refinement of moist adiabatic adjustment toward a more realistic thermodynamic structure. Considerable work needs to be done to test and develop these ideas further.

Section 2 introduces the basic application of SP methods to diabatic and mixing processes, the definitions of θ_v using the SP, and the use of SP diagrams to

study boundary layer equilibrium. Section 3 presents illustrative examples of convective thermodynamic structure and Section 4 proposes an SP adjustment procedure as a parametric method for moist convection.

2. SATURATION POINT THERMODYNAMICS

2.1 The Saturation Point

Fig. 1 shows three lines representing the conservation of three variables (θ, θ_E, q) for unsaturated air and (θ_L, θ_{ES}, q_T) for cloudy air which intersect at a point, where the temperature and pressure (T_{SL}, p_{SL}) completely specify the three conserved parameters, which we shall represent by θ_{SL}, θ_{ESL} and q_{SL}. We shall call this point the Saturation Point (SP) and the pressure level at which it occurs the Saturation Level (SL).

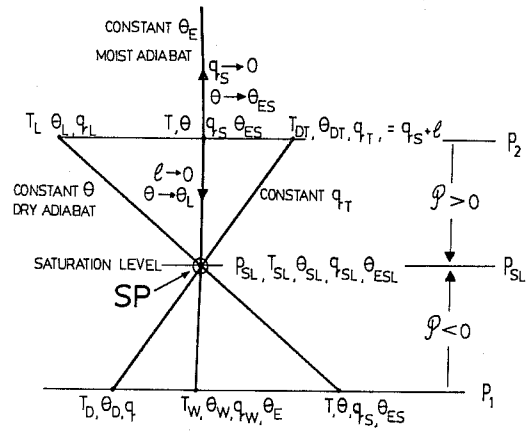

Fig. 1 Sketch thermodynamic diagram (tephigram), showing the relationship of Saturation Point SP (T_{SL}, p_{SL}) to the conserved parcel properties (θ_{SL}, θ_{ESL}, q_{SL}) which are independent of parcel pressure, and to the parcel properties at other pressure levels, such as (T, T_W, T_D) at p_1, for unsaturated air (for which $\mathcal{P} < 0$). The arrows on the moist adiabat denote the paths of integration in the definition of θ_{ES}, θ_L.

In this frame of reference, the thermodynamic state of an air parcel is specified by the Saturation Point properties (T_{SL}, p_{SL}) and its pressure difference from the Saturation Level, i.e.,

$$\mathcal{P} = p_{SL} - p. \qquad (1)$$

On a thermodynamic diagram, air parcels that have a given (T, p) may have SL's at any level, p_{SL}, depending on their total moisture content. Parcels with total moisture content $q_T > q_S(T, p)$ will be saturated and cloudy with $\mathcal{P} > 0$, while if parcel $q < q_S(T, p)$, it will be unsaturated with $\mathcal{P} < 0$. Positive $\mathcal{P}$ is directly related to liquid water content; negative $\mathcal{P}$ to subsaturation. Only cloud water is treated as a parcel property.

We shall call $\mathcal{P}$ the parcel saturation pressure departure and p the parcel level or data pressure level to distinguish it from the Saturation Level, p_{SL}. The procedure we shall use is to analyze parcel processes, including cloud-environment mixing and diabatic processes in terms of their Saturation Point. This is a shift to a (T_{SL}, p_{SL}, p) coordinate system for the three independent parcel variables, from (T, p, q) or (θ_L, θ_E, p). If parcel $p \neq p_{SL}$, the non-conservative parcel properties such as T, q_S, ℓ, $T_{\mathcal{P}}$, etc., can be recovered as in Fig. 1 by drawing the dry and moist adiabats and line of constant q through the SP to parcel pressure p.

Air can go up and down in atmospheric circulations, but its SP is a tracer of its thermodynamic origins. The SP does not change (only $\mathcal{P}$ changes) unless there are non-conservative processes acting on the parcel such as precipitation, evaporation of falling rain or radiational cooling. These can be regarded as constrained modifiers of the SP (see Fig. 2). Conceptually the SL also has a physical meaning: apart from these non-conservative processes, it is the pressure level where an air parcel last entered or left cloud.

2.2 Processes that move the SP

Fig. 2 summarizes various diabatic processes that move the SP in the two-dimensional field of a thermodynamic diagram.

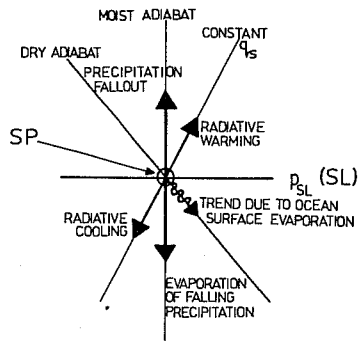

Fig. 2. Schematic showing change in saturation point produced by irreversible diabatic processes of precipitation fallout or evaporation; radiative cooling or heating; and the tendency caused by ocean surface evaporation.

Fallout of precipitation moves the SP up the moist adiabat. The air parcel θ_{ESL} does not change, but θ_{SL}, q_{SL} do, as ℓ decreases. For the special case of an air parcel at constant pressure, the parcel (T, p) remains constant as T_L, T_{DT} both approach T, while maintaining the relationship (as ℓ and $\mathcal{P} \to 0$)

$$C_p(T - T_L) = L\ell. \qquad (2)$$

This is exactly analogous to the evaporation of falling precipitation into unsatu-

rated air which moves the SP down the moist adiabat: again the parcel θ_{ESL} does not change, while θ_{SL}, q_{SL} do. If the parcel is at constant pressure, the T, T_D both approach the wet-bulb temperature T_W which remains constant, and $|\mathcal{P}|$ decreases toward zero. The relationship (2) is maintained, as T, T_D change toward T_W

$$C_p(T - T_W) = L(q_W - q) \qquad (3)$$

If the parcel pressure changes during the evaporation process, the behavior of the SP remains the same, although the parcel saturation pressure difference $\mathcal{P}$ changes. Betts and Silva Dias (1979) and Betts (1982b) discussed this process in detail.

Radiative processes change the temperature, but not the mixing ratio, so that θ_{ESL}, θ_{SL} change, while q_{SL} remains constant. In the free atmosphere there are no processes which change q_{SL}, while conserving θ_{SL}, although at the ocean surface this is the trend produced by the evaporation of water, using the stored sensible heat of the ocean. However, in this case the SP (here the LCL of cloud base) stays constant because the vertical advection of water vapor through cloud base balances the surface flux.

Although Fig. 2 is not drawn to scale, the thermodynamic balance of the entire tropical atmosphere can be regarded as a result of the approximate balance of the three processes: ocean surface evaporation, radiative cooling and precipitation fallout, each tending to move the SP in different directions. In section 3, we shall construct schematic 'vector' diagrams showing the balance of the various flux terms in the convective boundary layer.

2.3 Mixing processes and mixing lines

The parcel conserved parameters (θ_{SL}, θ_{ESL}, q_{SL}) are conserved in adiabatic motion and approximately in isobaric mixing processes (Betts, 1973; Deardorff, 1976, 1980). Since the SP characterizes parcel conserved properties, we need only consider their SP's in mixing two parcels. This is a great simplification.

Fig. 3 shows a specific example of mixing between two parcels with saturation points (T_{SL}, p_{SL}) of (20° C, 900 mb) and 5° C, 700 mb). The SP's of all mixtures (not just the mixture of equal masses) lie on the dashed mixing line, which can easily be constructed on a thermodynamic diagram by computing θ_{SL}, q_{SL} for different mixtures and finding their associated SP.

The distinction between the saturation level of a parcel p_{SL} and the data pressure level p, where a parcel may find itself in the atmosphere, is of crucial importance. The tephigram is being used to represent both. For example, suppose we consider a mixing process at 800 mb between cloudy air which has risen adiabatically from cloud base at 900 mb where it had the SP at C shown. Its SP has stayed at C, while $\mathcal{P} = p_{SL} - p$ has become positive and its liquid water has increased. This cloudy air mixes isobarically at 800 mb with air that has an SP at E (unsaturated environmental air, for example, which could have originated at 800 mb or descended

adiabaticallyfrom any other level). All the mixtures of C and E have SP's on the dashed line. The mixtures that are unsaturated have a saturation level $p_{SL} < 800$ mb, correspondingly to $\mathcal{P} < 0$, while the mixtures that are cloudy are those which have $p_{SL} > 800$ mb. The 1:1 mixture in Table 1, for example, with SL at 804 mb, is only just cloudy at 800 mb; if it sinks to pressures above 804 mb, it becomes unsaturated. Its (T, T_W, T_D) or (T_L, T, T_{DT}) at any other pressure level are found by drawing dry and moist adiabats and constant q_S lines through its SP as shown (the same construction as in Fig. 1).

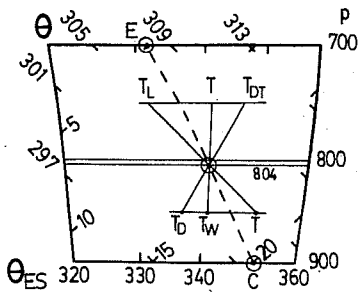

Fig. 3 Tephigram showing mixing between parcels with SP's at C and E (circled). All mixtures have SP's on the dashed mixing line. The 1:1 mixture has SP (T_{SL}, p_{SL}) at (13.5° C, 804 mb) shown. This gives its conserved parameters: Its parcel properties at other pressure levels are given by the construction shown.

The dashed line, representing the SL's and SP's of all mixtures (of C and E) is unchanged, whatever the pressure level of mixing; although for every mixture $\mathcal{P}$ changes as p changes.

Convective mixing plays an important role in determining atmospheric structure. In some casesthe vertical thermodynamic structure approaches in equilibrium a mixing line, while in others it can be analyzed in terms of processes moving it away from the equilibrium state (see Sections 3, 4).

2.4 θv isopleths

The virtual temperature correction is important to analyses of instability and convective equilibrium. θ_v overlays can be drawn for a thermodynamic diagram in terms of SP coordinates. For unsaturated air

$$\theta_{vu}\,(p_{SL}) = \theta_{SL}(1 + 0.61\, q_{SL}) \qquad (4)$$

and θ_{vu} is a function only of the air parcel SP. For cloudy air, with cloud water content ℓ

$$\theta_{vc}(p_{SL}, p) = \theta(p)\left[1 + 0.61\, q_S(p) - \ell(\mathcal{P}_c)\right] \qquad (5)$$

so that θ_{vc} like θ is a function of both parcel pressure (which is the pressure level where θ, q_S are defined) and the saturation level (which determines total water, and hence ℓ). Diagrammatically this means the θ_v isopleths, which are read at the SP, kink at the parcel pressure p (Fig. 6), since parcels for which $p_{SL} < p$ are unsaturated, while those for which $p < p_{SL}$ are cloudy.

Fig. 4 is a section of a low-level tephigram with θ_v isopleths (heavy dashes) overlaid for a parcel level of 850 mb. For SL's $p_{SL} < 850$ mb (the "unsaturated region"), θ_{vu} increases along the dry adiabat ED (for example) as the saturation mixing ratio ($q_S = q_{SL}$) increases, while for $p_{SL} > 850$ mb ("the cloudy region"), SP's on the moist adiabat BC have the same θ, q_S at point B, but decreasing θ_{vc} as ℓ increases on BC.

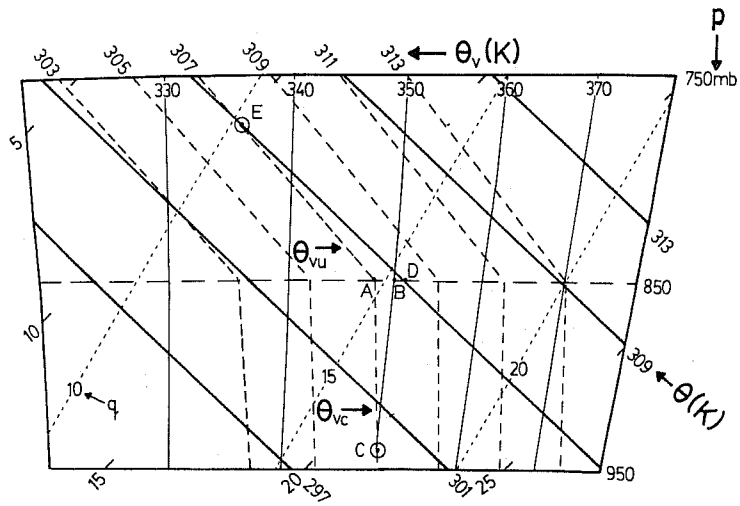

Fig. 4. Section of tephigram showing isopleths of θ_v (heavy dashed, in degrees K) for a parcel level of 850 mb. The light dashed lines are saturation mixing ratio.

If an air parcel moves from 850 mb dry or moist adiabatically to another pressure level, its SP does not change, but the isopleths now kink at another p level. If the parcel remains unsaturated θ and θ_{vu} are unchanged, but if the parcel is cloudy, both θ and θ_{vc} change.

It is the slopes of the θ_v isopleths that are important for stability analyses. We shall express these slopes as a fraction of the moist adiabat $\Gamma_W = (\partial\theta/\partial p)_{\theta_{ES}}$. For unsaturated air, we may write the slope of the θ_{vu} isopleth:

$$\left(\frac{\partial\,\theta_{SL}}{\partial\,p_{SL}}\right)_{\theta_{vu}} = \beta_1\,\Gamma_W \qquad (6a)$$

where β_1 increases from 0.12 to 0.24 as q_S increases from 5 to 20gKg^{-1}. (Betts, 1982a) For cloudy air, the deviation of the θ_{vc} isopleth from the moist adiabat may

be written:

$$\Gamma_W - \left(\frac{\partial \quad SL}{\partial \quad p_{SL}}\right)_{\theta_{vc},\ p} = \beta_2 \Gamma_W \simeq 0.1 \qquad (6b)$$

where the coefficient β_2 is nearly independent of q_S. The practical significance of is that although an ascending cloud parcel θ follows the moist adiabat, its buoyancy is effectively following a θ_{vc} isopleth with slope $0.9\,\Gamma_W$, until cloud water is precipitated - a considerable reduction in buoyancy (well known to cloud modellers!).

Just as θ changes in moist adiabatic processes, but θ_{ES} does not, we can define a θ_{ESV} which is a function only of SP for cloudy parcels and use this as a more conservative label for the θ_{vc} isopleths.

Deardorff (1976, 1980a) showed how θ_{vc} perturbations can be expressed as linear combinations of conserved parameters. In SP notation

$$\theta_{vc} = \eta_1 \delta\theta_{ESL} - \theta\delta q_{SL}, \qquad (7)$$

where

$$\eta_1 = \theta(1 + 1.61\alpha)/(1 + L\alpha/C_pT)\,\theta_{ES}$$

$$\alpha = T dq_S/dT.$$

Rearranging (8) permits a definition of an isopleth of virtual θ_{ES}

$$0 = \delta\theta_{ESV} = \delta\theta_{ESL} - \theta_{ES}\, q_{SL}/\eta_2, \qquad (8)$$

where

$$\eta_2 = \frac{\theta_{ES}}{\theta}\,\eta_1 .$$

These θ_{ESV} isopleths have the same slope as the θ_{vc} isopleths: 0.9 of the moist adiabat. Betts (1983) labelled the θ_{ESV} isopleths at 1000 mb by integrating (8)

$$\theta_{ESV} = \theta_{ES}(p) + \int_{q_S}^{q_S(1000)} (\theta_{ES}/\eta_2)\, dq_{SL}. \qquad (9)$$

The significance of the θ_v isopleths is that they are reference processes related to stability and characterize dry and cloudy convective processes in the atmosphere. For all analyses of buoyancy it is the θ_{vu}, θ_{ESV} isopleths not the dry and moist adiabats that are important. We shall see (Section 4) that highly disturbed convective atmospheres approach a θ_{ESV} structure in the low troposphere.

2.5 Boundary layer equilibrium: SP diagrams

In zones of subsidence, mixed layer or subcloud SP can be found from a balance of surface fluxes, radiative divergence and the divergence at the subsidence inversion. The convection can be regarded as a mixing process between the surface and the free atmosphere, and subcloud layer SP can be found from a simple SP vector difference diagram.

2.5.1 Boundary layer budget schematic

We shall consider a steady (horizontally homogeneous) equilibrium structure (over an

ocean surface), and assume $\bar{\omega}$ constant above the subcloud layer for simplicity (Fig. 5). The thermodynamic budget equation for the whole convective layer is

$$\Delta p \frac{d\bar{\underset{\sim}{S}}}{dt} = 0 = g\underset{\sim}{F}_o + \bar{\omega}(\underset{\sim}{A} - \underset{\sim}{B}) + g\Delta\underset{\sim}{R}$$

where $\Delta\underset{\sim}{R}$ is the radiative flux divergence across the boundary layer (B L), $\underset{\sim}{A}$ is the SP of air sinking into the BL, $\underset{\sim}{B}$ is subcloud layer SP, and $\bar{\underset{\sim}{S}}$ a vertically averaged SP for the BL. The surface flux can be parameterized $\underset{\sim}{F}_o = \omega_o(\underset{\sim}{Q} - \underset{\sim}{B})$ where $\omega_o = \rho g C\bar{V}$ is related to the surface wind speed $\bar{V}$ and a surface bulk transfer coefficient C. Thus

$$0 = \omega_o(\underset{\sim}{Q} - \underset{\sim}{B}) + \bar{\omega}(\underset{\sim}{A} - \underset{\sim}{B}) + g\Delta\underset{\sim}{R} \qquad (10a)$$

This balance gives the subcloud layer SP ($\underset{\sim}{B}$). Formally we may consider an equilibrium state B' without radiative divergence $\Delta\underset{\sim}{R}$, which satisfies

$$0 = \omega_o(\underset{\sim}{Q} - \underset{\sim}{B}') + \bar{\omega}(\underset{\sim}{A} - \underset{\sim}{B}') \qquad (10b)$$

B' lies on the mixing line between the surface $\underset{\sim}{Q}$ and the free atmosphere $\underset{\sim}{A}$ such that it divides $(\underset{\sim}{Q} - \underset{\sim}{A})$ in the ratio $\bar{\omega}/\omega_o$.

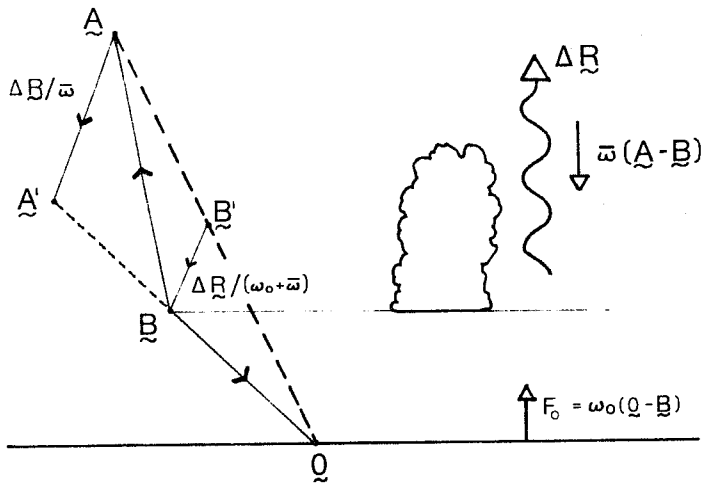

Fig. 5. SP structure for a convective boundary layer in equilibrium showing the balance of surface fluxes, subsidence and radiative cooling. $\underset{\sim}{B}$ is subcloud layer SP.

Subtracting (10a) and (10b) gives the deviation of B from B'

$$(\underset{\sim}{B} - \underset{\sim}{B}') = \Delta\underset{\sim}{R}/(\omega_o + \bar{\omega}) \qquad (11)$$

so that $\underset{\sim}{B}$ lies off the mixing line $\underset{\sim}{Q}$ $\underset{\sim}{A}$ along a line of constant q_s a distance related to the radiative divergence. $(\underset{\sim}{B} - \underset{\sim}{B}')$ is along a line of constant q_s through $\underset{\sim}{B}'$. An equivalent description is to modify $\underset{\sim}{A}$ to $\underset{\sim}{A}'$ such that $(\underset{\sim}{A}' - \underset{\sim}{A}) = \Delta\underset{\sim}{R}/\bar{\omega}$. Then $\underset{\sim}{A}'$ $\underset{\sim}{B}$ $\underset{\sim}{Q}$ is a mixing line.

I have not yet fully explored the shallow cumulus structure, but Betts (1983) does present solutions for a mixed stratocumulus layer, so I'll discuss this case in a little more detail.

2.5.2 Steady-state stratocumulus (from Betts, 1983)

Betts (1983) shows that the constant fluxes in the mixed layers can be parameterized at the surface, in the mixed layer and at cloud-top using the SP notation (Figs. 6, 7) as

$$g\underset{\sim}{F} = \omega_o(\underset{\sim}{O} - \underset{\sim}{M}) = \omega^*(\underset{\sim}{A} - \underset{\sim}{D}) = \omega_T(\underset{\sim}{M} - \underset{\sim}{T}') \qquad (12)$$

where $\omega_o = \rho g C \overline{V}$ (C is a bulk aerodynamic transfer coefficient at the surface; ω^* is the convective mass circulation; ω_T, the cloud-top subsidence = ω_e the entrainment velocity, and

$$g\underset{\sim}{R} = \omega_T(\underset{\sim}{T} - \underset{\sim}{T}') \qquad (13)$$

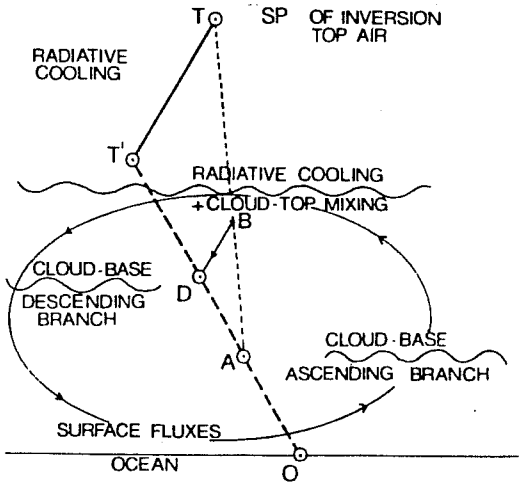

Fig. 6. Schematic for steady-state, well-mixed stratocumulus over the ocean showing saturation point diagram, and cloud-bases for ascending and descending branches of a single-cell circulation

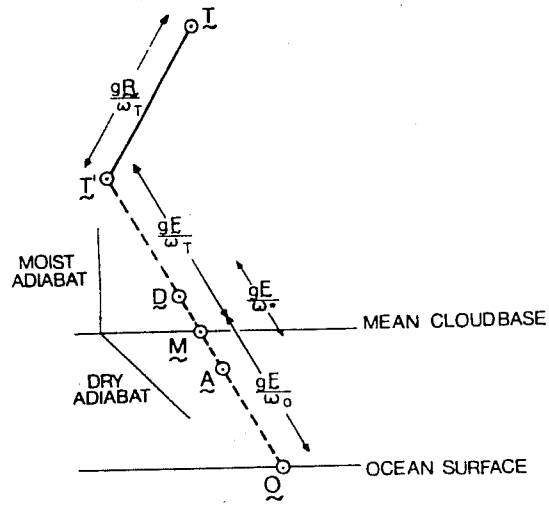

Fig. 7. (As Fig. 1) The heavy dashed line is a mixing line. $\underset{\sim}{T}\,\underset{\sim}{T}'$ is the radiative modification of inversion-top SP along a line of constant q_S. The relation between fluxes and SP differences are as shown.

Solving (12) for the mixed layer SP, $\underset{\sim}{M}$, (Schubert, 1976) gives

$$\underset{\sim}{M} = \frac{\omega_o \underset{\sim}{O} + \omega_T \underset{\sim}{T}'}{\omega_o + \omega_T} \qquad (14)$$

Parallel expressions exist in terms of $\underset{\sim}{A}$, $\underset{\sim}{D}$, ω^*. It is clear that with the constant flux assumption (steady state) and the representation of the cloud-top radiative divergence as a single modification of inversion top air (T to T'), then SP's within the mixed layer are then simple averages (weighted by combinations of the characteristic velocities) of the end points $\underset{\sim}{O}$, $\underset{\sim}{T}'$. It follows that the four SP's $\underset{\sim}{O}$, $\underset{\sim}{A}$, $\underset{\sim}{D}$, $\underset{\sim}{T}'$ lie on one mixing line, and that processes within the mixed layer can be represented diagrammatically as mixing processes.

2.5.3 Parameterization of surface fluxes

Another arrangement of (1) gives the surface fluxes in terms of differences across the layer

$$g\underset{\sim}{F} = \left(\frac{\omega_T \, \omega_0}{\omega_T + \omega_0}\right)(\underset{\sim}{0} - \underset{\sim}{T}') \qquad (15)$$

which represents the surface fluxes of θ, q, θ_E.

The determination of the surface fluxes for the steady-state stratocumulus layer thus requires surface parameters ω_0, $\underset{\sim}{0}$ (the SP of surface air), and a set of cloud-top parameters, $\underset{\sim}{T}$, ω_T, $\underset{\sim}{R}$ (which determine $\underset{\sim}{T}'$ through (2).

2.5.4 Buoyancy, θ_v fluxes, and convective available potential energy (CAPE)

Betts (1982a, 1983a) show how θ_v isopleths can be used on SP thermodynamic diagrams to discuss buoyancy and CAPE. The construction for the constant flux stratocumulus layer is shown in Fig. 8. $\underset{\sim}{0}\ \underset{\sim}{A}\ \underset{\sim}{D}\ \underset{\sim}{T}$ is the mixing line as in Fig. 7. $\theta_{vc}(\theta_{ESV})$ isopleths (for unsaturated and cloudy air) are drawn through $\underset{\sim}{A}$, $\underset{\sim}{D}$, the SP's of the ascending and descending branches of the circulation.

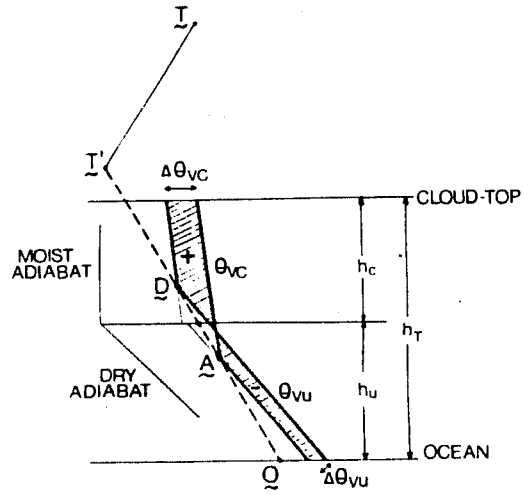

Fig. 8. Construction of convective available potential energy (shaded area) using θ_v isopleths through SP's of ascending and descending branches for steady-state stratocumulus over a (cold) ocean. Mixed layer depth is h_T:h_c, h_u are the mean pressure thicknesses for the cloud and subcloud (unsaturated) layers respectively.

The criterion for no cloud-top entrainment instability (Randall, 1980; Deardorff, 1980) is that $\underset{\sim}{A}\ \underset{\sim}{T}$ lies to the right of the θ_{vc} isopleth (Betts, 1982a). This criterion is satisfied in Fig. 8, so that cloud-top mixing alone does not produce freely entraining negatively buoyant downdrafts. Instead there is a slower circulation in which cloudy mixtures become negatively buoyant at cloud-top by radiative cooling of $\underset{\sim}{T}$ to $\underset{\sim}{T}'$, together with mixing to give $\underset{\sim}{D}$. For a direct thermal circulation in the cloud layer (driven that is by radiative cooling), we require the mixing line $\underset{\sim}{0}\ \underset{\sim}{A}\ \underset{\sim}{D}\ \underset{\sim}{T}'$ to lie to the left of the θ_{vc} isopleth through $\underset{\sim}{A}$, so that $\Delta\theta_{vc}$ is positive as shown. Conversely in the subcloud layer (below $\underset{\sim}{A}$), Fig. 8 shows $\Delta\theta_{vu}$ negative, which means the ascending branch has negative buoyancy and the subcloud circulation is (in the case shown) an indirect one driven by the available potential

energy converted in the cloud layer. Since the circulation as a whole must be energy generating, there is a constraint on $\Delta\theta_{vc}$, $\Delta\theta_{vu}$ which determines the slope of the mixing line $\underset{\sim}{O}\ \underset{\sim}{A}\ \underset{\sim}{D}\ \underset{\sim}{T}'$ from the dissipation of the circulation kinetic energy (see Betts, 1983).

2.5.5 SP vector diagram for unsteady mixed stratocumulus

The SP vector diagram can be used to describe the approach to equilibrium of a time-dependent layer (M not constant). The mixed layer budget equation can be written

$$h_T \frac{d\underset{\sim}{M}}{dt} = \omega_o(\underset{\sim}{O} - \underset{\sim}{M}) - \omega_e(\underset{\sim}{M} - \underset{\sim}{T}') \qquad (16)$$

where h_T is the pressure depth of the mixed layer (surface to cloud-top), and the entrainment velocity at cloud-top satisfies:

$$\omega_e = \frac{dh_T}{dt} + \omega_T$$

The radiative flux divergence at cloud-top still satisfies (13). If we now define an equilibrium state, E, by

$$0 = \omega_o(\underset{\sim}{O} - \underset{\sim}{E}) - \omega_e(\underset{\sim}{E} - \underset{\sim}{T}') \qquad (18)$$

then substracting the vector equations (16), (17) gives

$$h_T \frac{d\underset{\sim}{M}}{dt} = (\omega_o + \omega_e)(\underset{\sim}{E} - \underset{\sim}{M}) \qquad (19)$$

Equation (19) expresses the tendency of the layer mean SP in terms of an SP difference from equilibrium ($\underset{\sim}{E}$ - M) and an adjustment time scale for the layer

$$\tau = h_T(\omega_o + \omega_e) \qquad (20)$$

Fig. 9 shows the SP vector diagram.

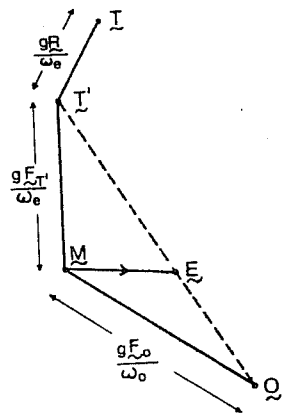

Fig. 9. Saturation Point vector diagram for unsteady mixed stratocumulus layer. The mixed layer SP, $\underset{\sim}{M}$, has an (instantaneous) tendency toward $\underset{\sim}{E}$ on the dashed mixing line between $\underset{\sim}{O}$ $\underset{\sim}{T}'$.

These diagrams relate the boundary layer structure and time dependence to surface parameters, those in the free atmosphere and the radiative fluxes. I believe a general boundary layer parameterization can be most economically formulated by comparing these SP schematics, to observational data sets, so as to determine the key closure parameters.

3. ILLUSTRATIONS OF CONVECTIVE STRUCTURE

3.1 Mixed convective equilibrium: the cumulus layer

Cumulus convection is a moist mixing process between the subcloud layer and drier air aloft, and not surprisiningly the thermodynamic structure tends toward a mixing line.

3.1.1 Mixing line structure

Fig. 10 shows the (T, T_D) structure (solid lines) and corresponding SP's (open circles) from the surface to 700 mb for a late afternoon convective sounding over land in the tropics. The entire SP structure from 980 mb to 700 mb lies close to the mixing line joining the end-points. There is a patch of cloud near 750 mb and a dry layer above, but these large fluctuations of T and T_D only appear as SP fluctuations up and down the mixing line.

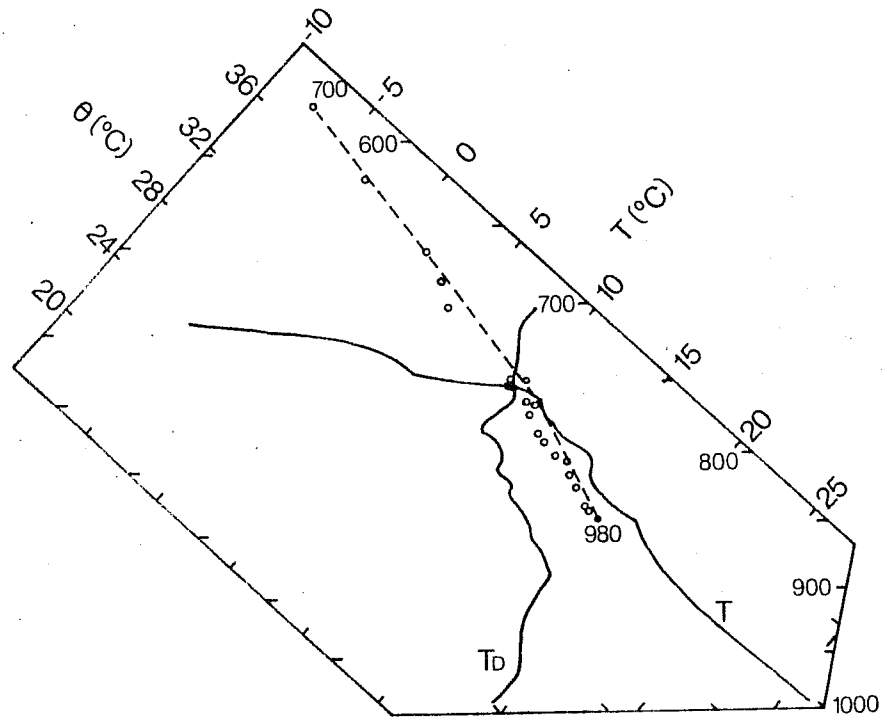

Fig. 10. Late afternoon convective structure, showing SP's lying along a mixing line (Venezuela, 1972, sonde 99).

3.1.2 Trade cumulus equilibrium: balance of convective mixing and radiation

Fig. 11 shows a three-day BOMEX average for the undisturbed Tradewinds. The dashed line is the mixing line between cloud-base air and subsiding air just above the trade inversion. We note

(i) The mixing line is well to the left of the stratocumulus breakup criterion.

(ii) Above the base of the trade inversion, just saturated mixtures are cold and will readily sink in downdrafts to the base of the inversion.

(iii) The lapse rate in the conditionally unstable cumulus layer is very close to the mixing curve (cf. Fig. 10), which does not favor downdrafts in this layer. This and other examples suggest that the lapse rate in the lower cumulus layer is controlled by the mixing process.

(iv) However, SP's of the environment in the cumulus layer lie to the left of the mixing line. This cannot be explained by mixing alone and indicates radiative cooling is involved in the equilibrium (schematically shown by arrows).

The boundary layer model from Section 2 can be extended to quantitatively describe the cloud-layer balance of convective transports and radiative cooling.

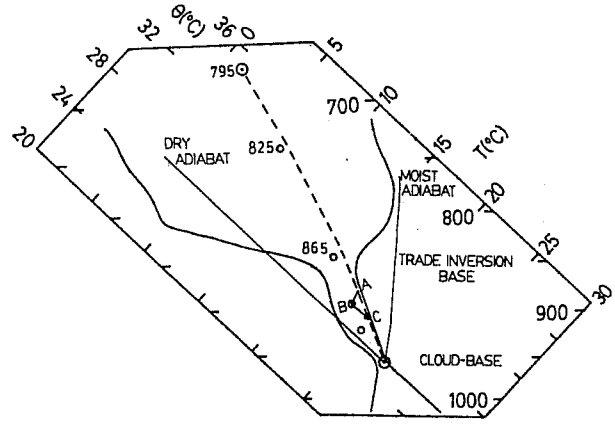

Fig. 11. Three-day average sounding for undisturbed tradewind convection (BOMEX 22-24, June, 1969). Heavy dashed line is mixing line between inversion top, and cloud-base air.

Consider a horizontally homogeneous trade cumulus boundary layer whose mean structure is shown by Fig. 12. We now distinguish the cloud layer separately. In equilibrium (taking $\bar{\omega}$ constant in the cloud layer)

$$0 = g\underset{\sim}{F}_B + \bar{\omega}(\underset{\sim}{A} - \underset{\sim}{C}) + g\Delta\underset{\sim}{R}_c$$

where $\underset{\sim}{F}_B = \omega^*(\underset{\sim}{B} - \underset{\sim}{C})$ is the cloud-base convective flux; $\underset{\sim}{C}$ is the environmental mean SP at cloud-base, and $\Delta\underset{\sim}{R}_c$ is the radiative flux divergence for the cloud layer. A parallel analysis to Section 2.5 shows that $\underset{\sim}{C}$ lies of the $\underset{\sim}{A}$ $\underset{\sim}{B}$ mixing line because of $\Delta\underset{\sim}{R}_c$, such that

$$(\underset{\sim}{C} - \underset{\sim}{C}') = \Delta\underset{\sim}{R}_c/(\omega^* + \bar{\omega})$$

where $\underset{\sim}{C}'$ divides the mixing line $\underset{\sim}{A}$ $\underset{\sim}{B}$ in the ratio $\omega^*/\bar{\omega}$. As before, this can alternatively be described by first modifying $\underset{\sim}{A}$ to $\underset{\sim}{A}''$ by $\Delta\underset{\sim}{R}_c/\bar{\omega}$ and then finding $\underset{\sim}{C}$ on $\underset{\sim}{A}''$ $\underset{\sim}{B}$.

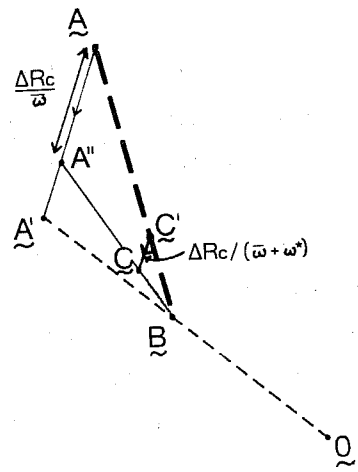

Fig. 12. SP structure of trade-cumulus cloud-layer, showing balance of cloud-base flux, subsidence and radiative cooling in the cloud layer.

The BOMEX data fits this type of model quantitatively although the details are sensitive to the humidity corrections applied to the data (Betts, 1982a).

3.1.3 Convective boundary layer over land

The shallow convective boundary layer over land is highly time-dependent since cloud base rises as the subcloud layer warms and (typically) dries under the influence of diurnal heating. Fig. 13 shows an example (from Betts, 1976) of the mean change from 1000 to 1400 local time over Venezuela. The data is an average of sounding pairs from 20 days convection. The T and SP profiles are shown for the two sounding times. The temperature profile shows an dry adiabatic structure to cloud-base and essentially a θ_{ESV} structure above cloud-base, which is maintained as cloud-base rises. The arrows show the change of SP at each pressure level from 1000 to 1400. Below cloud-base there is a warming and drying; above cloud-base primarily a moistening. The dashed lines are mixing lines from the SP of 650 mb air to cloud-base for the two times. The sounding structures lie off these mixing lines, because of the time dependence, but a similar structure is maintained as cloud-base rises. A simple budget equation for a slice of the cloud layer is (neglecting radiative divergence)

$$\frac{\partial \underset{\sim}{\bar{S}}}{\partial t} = \frac{\partial \underset{\sim}{F}}{\partial p} + \bar{\omega}\partial \underset{\sim}{S}/\partial p$$

where $\underset{\sim}{F}$ is the convective flux: integrating through the cloud layer (thickness Δp) gives (taking $\bar{\omega}$ constant)

$$\Delta p \; \overline{d\underset{\sim}{S}/dt} = \omega^*_B(\underset{\sim}{B} - \underset{\sim}{C}) + \bar{\omega}(\underset{\sim}{A} - \underset{\sim}{C})$$

where ω^*_B is cloud-base mass flux, and $\underset{\sim}{A}$, $\underset{\sim}{C}$, $\underset{\sim}{B}$ are the SP's of the environment at cloud-top and cloud-base and of the subcloud layer respectively. For this data set $\omega^* >> \bar{\omega}$ (Betts, 1976) and the cloud-base difference $(\underset{\sim}{B} - \underset{\sim}{C})$ is related to a time-scale

$$(\underset{\sim}{B} - \underset{\sim}{C}) = \mathcal{P}\overline{d\underset{\sim}{S}/dt} \quad \text{where} \quad \mathcal{P} = \Delta p/\omega^*_B$$

In the cloud layer $\mathcal{P}$ is reduced by the convection from $\sim$ -60 mb to $\sim$ -35 mb. The dashed mixing lines have a BOWEN Ratio $\sim$ -0.5.

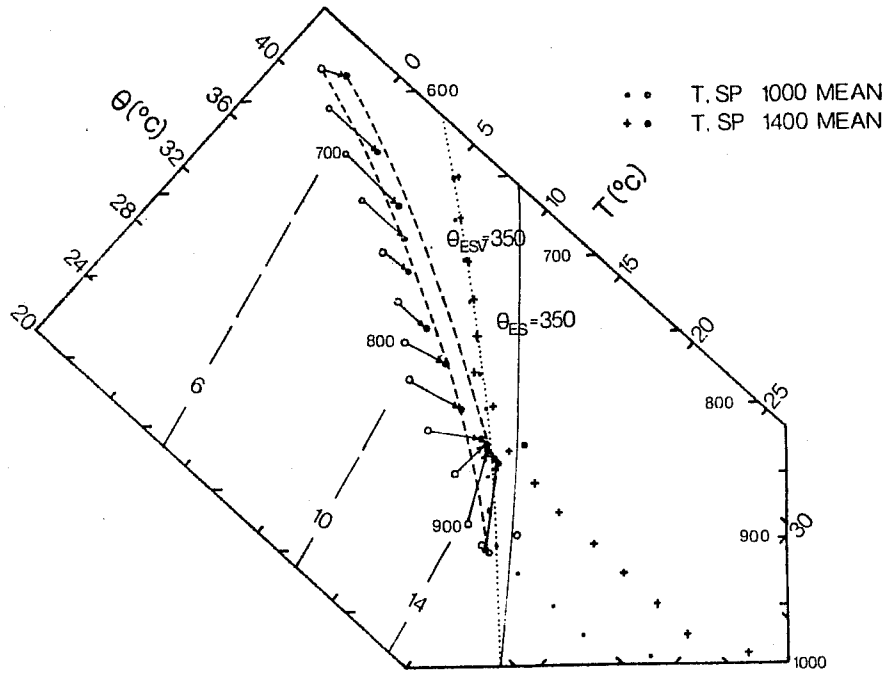

Fig. 13. Temperature and SP structure of mean soundings over land showing local change (1000 to 1400 local time). Dotted line is θ_{ESV} isopleth, dashed lines are mixing lines.

3.2 Transitions between air masses

It is useful to constrast how the SP structure shows up discontinuities between air masses which are not convectively mixed. An example is given from GATE in Fig. 14 in which a nearly moist adiabatic SP structure overlies a drier mixing line structure. Three soundings from nearby ships all show the same air mass transition.

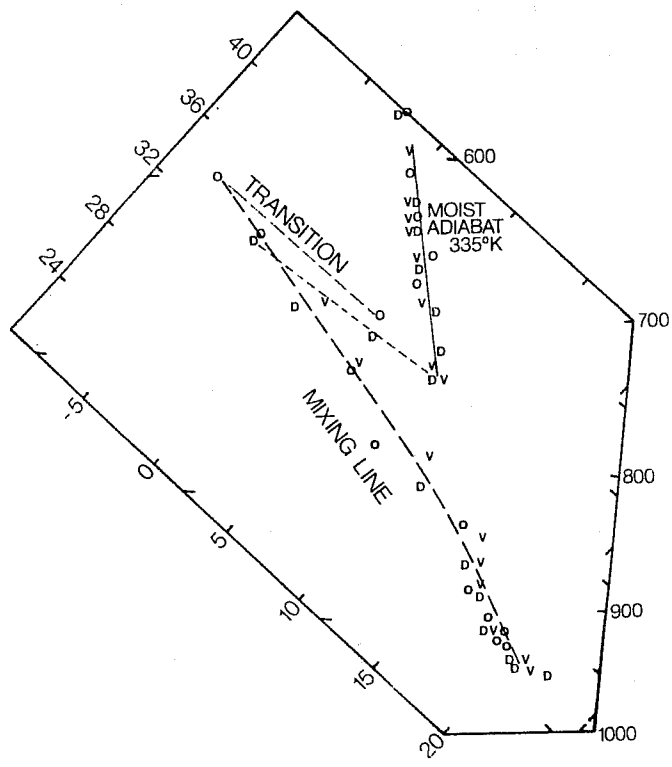

Fig. 14. Soundings at Oceanographer, Vanguard and Dallas on GATE day 258 showing transition between different atmospheric layers.

3.3 SP structure of a day's convection

If simply the SP structure of a sounding is plotted, one may compactly represent the thermodynamic structure of many soundings. Figs. 15, 16 show examples for two rainy days' convection: one from VIMHEX, one from GATE, which are quite similar. All the soundings cluster near to a mixing line structure. Different days, however, often have different characteristic SP structures. The mean slope, $d\theta_{ESL}/dp_{SL}$, of the mixing line is probably an important parameter, since it is related to the coupling of the convective fluxes of θ_L and q_T.

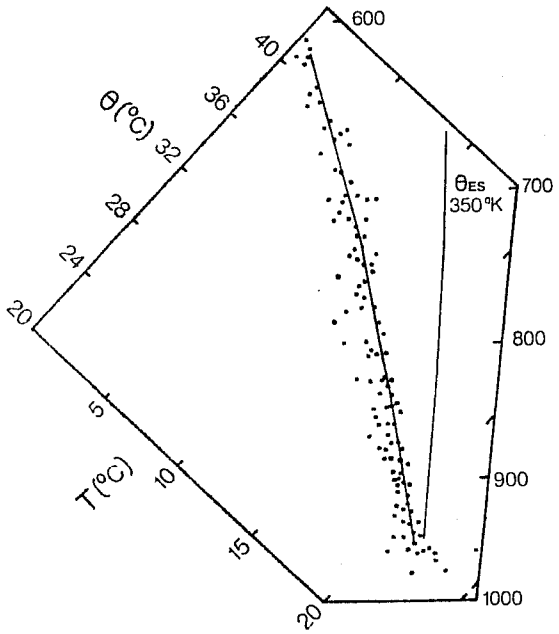

Fig. 15. SP structure of seven sequential soundings (over 11 hours) on a day with precipitation over Venezuela, showing mixing line structure (Aug. 9, 1972).

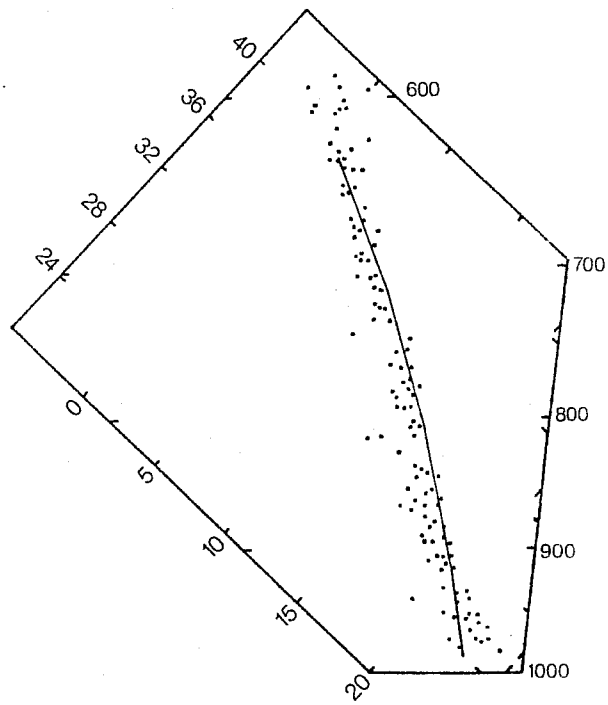

Fig. 16. Sequence of nine (three hourly) soundings at ship Dallas in GATE showing mean SP structure. (18Z Day 244 to 21Z Day 245).

3.4 Deep convective equilibrium

3.4.1 Tropical soundings over the ocean

Fig. 17 shows the structure of the deep troposphere for the mean typhoon sounding from Frank (1977). The heavy dots and open circles are (T, SP) for the eyewall. They show a θ_{ESV} structure below 600 mb and θ_{ES} increasing above, with a nearly saturated atmosphere ($\mathcal{P} \sim -15$ mb). The crosses and symbols E are (T, SP) inside the eyewall. Here the strong subsidence has produced a very stable thermal structure, but the SP structure is very close to the temperature structure of the eyewall: it has been generated by subsidence of air originally saturated at the eyewall temperature (this does not modify the SP). The mid-tropospheric subsidence within the eye is 60 mb. Thus the temperature structure of the eyewall is confirmed by two independent composites.

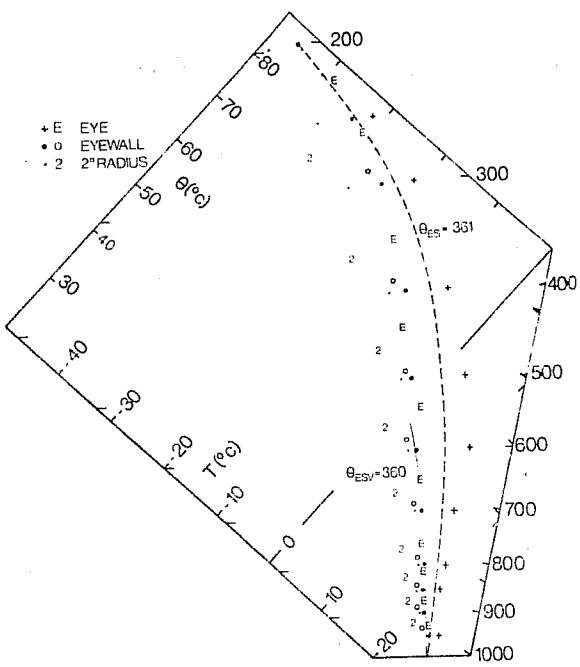

Fig. 17. Composite typhoon soundings inside the eye, the eyewall at 2° radius (Frank, 1977), showing T and SP structure.

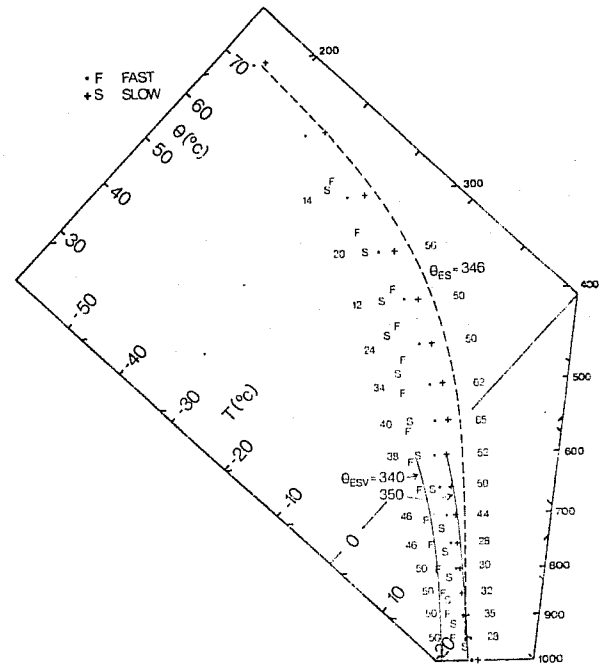

Fig. 18. Composite wake soundings for GATE slow and fast moving lines (Barnes, 1982), showing T, SP and $|\mathcal{P}|$ values.

The light dots and symbols 2 are the (T, SP) at 2° radius from the storm center. Here the atmosphere is further from saturation, but has a similiar cooler temperature structure. At 200 mb the eyewall $\theta_{ES} \sim 361$K, while at 2° radius $\theta_{ES} \sim 357$K, with a corresponding change in θ_E at the low levels.

Fig. 18 shows the deep tropospheric structure for the wake (Barnes and Sieckman, 1983) of GATE convective band composites. They show a very similar profile to Fig. 17, with an initial decrease of θ_{ES} close to a θ_{ESV} isopleth and then an increase above 600 mb (which is close to the freezing level). The dots and letter F denote the (T, SP) of fast-moving lines (Barnes and Sieckman, 1983) and the cross and letter S denote (T, SP) for slow-moving lines. They show some thermodynamic differences. The $|\mathcal{P}|$ values for each p level are shown (fast moving on left, slow on right). The fast-moving line wake has a drier lower troposphere (as a result of stronger downdrafts). Its 600 mb temperature is cooler, probably as a response to the falling θ_E in low levels. It is nearly saturated in the upper troposphere corresponding to extensive anvil clouds. The slow-moving line wake shows the reverse, with a moister lower tropospheric structure and θ_{ES} to 600 mb more closely aligned along a θ_{ESV} isopleth. It, however, is drier in the upper troposphere.

These thermodynamic differences are associated with distinct dynamic features in the wind profile: the fast-moving lines have strong shear between the surface and 650 mb (Barnes and Sieckman, 1983).

3.4.2 Convective equilibrium over land

Figs. 19, 20 show examples of average soundings of days of major convective episodes over land (Venezuela, 1972). The dots are the temperature structure and the open circles the corresponding SP's. The low-level T structures closely parallel a θ_{ESV} isopleth to the freezing level (near 600 mb) and then show an increase of θ_{ES} above. This structure is typical of deep convection in the tropics and may be regarded as more representative of deep convective equilibrium than say a moist adiabatic T structure. These days do not have fast-moving mesosystems.

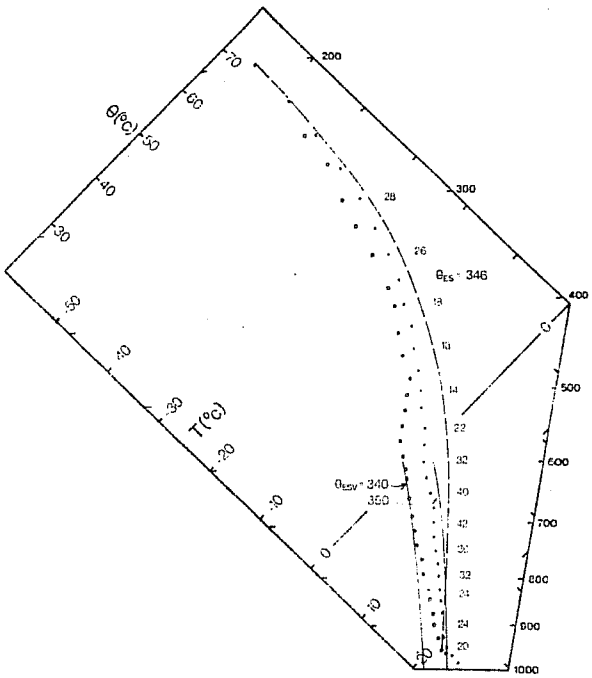

Fig. 19. Composite sounding for Aug. 9, 1972 (VIMHEX, 1972) showing T, SP structure (average of 7 soundings).

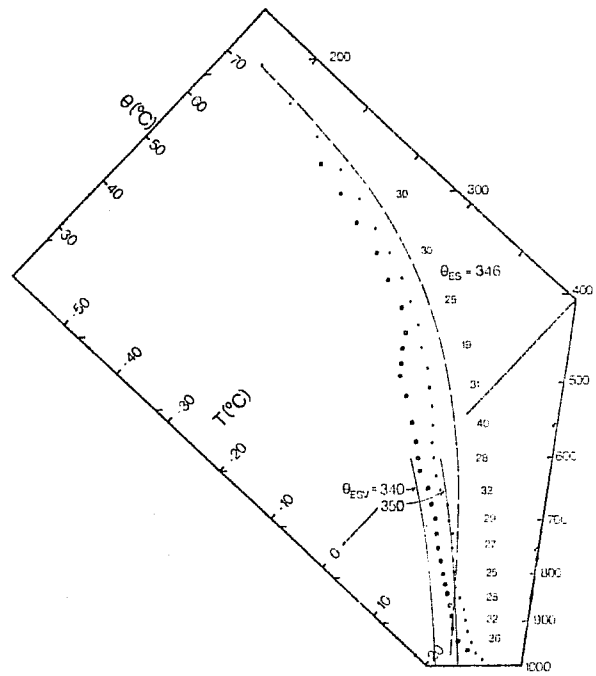

Fig. 20. As. Fig. 19 for Sept. 2, 1972 (6 soundings).

3.4.3 Fast-moving storms over land

Fig. 21 shows the inflow and outflow T, SP for a composite of fast-moving storms over Venezuela (Miller and Betts, 1977). Above 600 mb the upper tropospheric temperature structure is similar to Figs. 17-20. The low-level structure shows a marked drying and cooling of the deep subcloud layer to give values of p_B -50mb very similar to the GATE fast-moving composite, and a low-level outflow SP profile which is close to $\theta_{ESV} \sim 344K$.

3.5 Deep convective equilibrium structure -- parametric philosophy

Most tropical cumulonimbus have small vertical velocities ($\sim 10 m.s^{-1}$) (Zipser and Lemone, 1980), and must therefore have correspondingly small mean buoyancy excesses

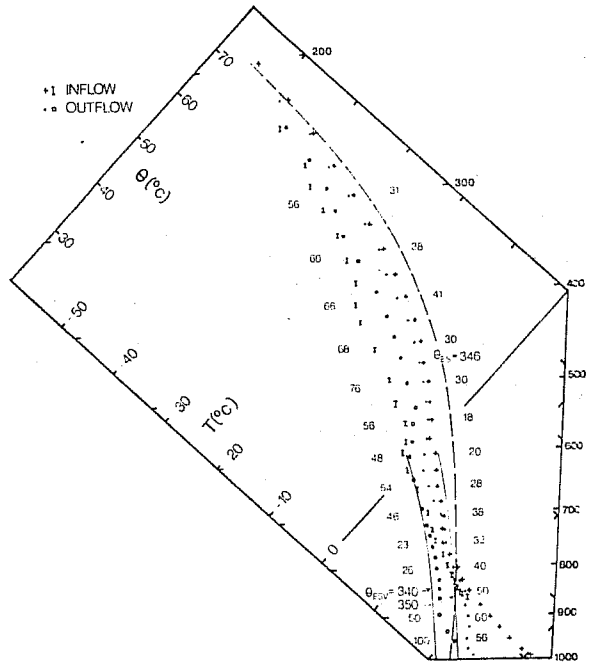

Fig. 21. Profiles of T, SP for inflow and outflow of a Venezuela composite of fast-moving storms (Miller and Betts, 1977).

(∿0.3K). Traditionally it has been assumed that temperatures on the moist adiabat are representative of parcel buoyancy for unmixed parcels, but this gives estimates for convective available potential energy far in excess of observed vertical kinetic energies. The θ_{ESV} isopleth which allows for the buoyancy correction for cloud water has a slope $d\theta/dz$ only 0.9 of that of the moist adiabat: a marked reduction in buoyancy in the low levels (Betts, 1982a). However, detailed computation of cloud parcel buoyancy allowing for fallout and partial freezing would require an elaborate cloud model. We shall adopt a different strategy for parametric purposes. If we assume that quasiequilibrium means that cloud-environment buoyancy differences become small in regions of active deep convection, then the environmental profile will reflect the cloud-scale processes which alter cloud-parcel buoyancy. Even though we cannot explain (in terms of a cloud model) all the detailed structure, we can use the observed thermodynamic structure as the basis for a parametric adjustment procedure. This seems preferable to attempting to generate in a numerical simulation a realistic quasiequilibrium structure by the use of cloud models (whether simple or complex).

To the extent that we can distinguish observationally differences in thermodynamic structure (and cloud fields) for dynamically different types of convection, these could be included in a parametric procedure.

3.6 Summary of observed convective equilibrium structure

Figs. 17-21 suggest that there is a tendency for deep convection to establish a quasiequilibrium thermodynamic structure, but that there are also some observable differences between dynamically different convective systems. All (even the nearly saturated hurricane eyewall convection) shows a marked decrease of θ_{ES} below 600 mb which is the approximate freezing level for this tropical set of data. The temperature structure approximates a θ_{ESV} isopleth suggesting that the lifting of cloud water is a significant density convection in active convective cells in the first few hundred mb above cloud base. The fast-moving storms show a more unstable θ_{ES} struc-

ture (Figs. 18, 21) and correspondingly a drier SP and $\mathcal{P}$ structure associated with stronger unsaturated downdrafts. Perhaps the rapid fall of low-level θ_E prevents a close approach to mid-level thermal equilibrium (see also below).

Around the freezing level both θ_{ES} and the SP show a marked stabilization with a steady increase of both in the upper troposphere toward the θ_{ES} isopleth through a low-level SP. This stable structure is probably associated both with freezing and the fallout of precipitation. Both increase cloud parcel buoyancy and we would expect this increase to be reflected in the mean sounding structure if the convection is not far from buoyancy equilibrium with the environment. Similarly the sounding minimums in θ_{ES} below the freezing level probably reflect both the buoyancy correction due to the lifting of cloud water in active cells and the melting of falling precipitation. That is, the θ_{ES} minimum is associated with both the lifting of precipitation and the melting/freezing couplet. The maintenance (in quasiequilibrium) of this profile requires an upward advection of θ_E by the convection. For a first guess parametric model we shall simply constrain θ_{ES} to have this minimum near the freezing level.

The $\mathcal{P}$ structure (related to subsaturation) shows more variability. Fast-moving storms with stronger downdrafts have $\mathcal{P} \sim -60$ mb in the low levels (related to a downdraft evaporation pressure scale, Betts 1982b) compared to $\mathcal{P} \sim -30$ mb in the low levels for the GATE show lines and VIMHEX August 9 and September 2 cases. Upper level values of $\mathcal{P}$ are variable in the -20 to -40 mb range: the smaller values (-20) correspond to layers closer to saturation. As a compromise and a first guess parametric scheme we shall use $\mathcal{P} = -30$ mb at all levels. This corresponds to a relative humidity of 85% at 800 mb and 75% at 500 mb.

4. SATURATION POINT ADJUSTMENT

4.1 Introduction

The idea is to specify a convective equilibrium state with SP structure $\underset{\sim}{E}(p)$ based on observations, and in the presence of (deep) convection, adjust the mean SP structure $\underset{\sim}{S}(p)$ toward this equilibrium state, $\underset{\sim}{E}$.

This work is in its infancy, and untested in models. Its main promise is that of maintaining a realistic convective thermodynamic structure and convective fluxes in the presence of large-scale forcing. It may be possible to extend the procedure to give a smooth transition for boundary layer clouds, and the development of stratiform clouds in mesoscale complexes.

4.2 Concept

The mean large-scale thermodynamic equations can be written in terms of SP, $\underset{\sim}{\bar{S}}$ as

$$\frac{\partial \underset{\sim}{\bar{S}}}{\partial t} = -\bar{V}.\nabla \underset{\sim}{\bar{S}} - \bar{\omega}\frac{\partial \underset{\sim}{\bar{S}}}{\partial p} - g\frac{\partial \underset{\sim}{R}}{\partial p} - g\frac{\partial \underset{\sim}{F}}{\partial p} \qquad (21)$$

where $\underset{\sim}{R}$, $\underset{\sim}{F}$ are the radiative and convective fluxes (components θ, q, θ_E fluxes).

In outline, the proposed procedure is

4.2.1 Allow large-scale mean fields plus radiation and surface fluxes to modify thermodynamic structure $\underset{\sim}{\bar{S}}$. Test for deep convection (moisture convergence) and cloud-top (θ_{ES} adiabat) (see 4.4).

4.2.2 Adjust back toward specified quasiequilibrium structure $\underset{\sim}{E}(p)$ which satisfies a θ_E conservation constraint (see 4.5) with a time-scale τ, representative of the convective time-scale.

If we abbreviate the large-scale forcing to the vertical advection we may write

$$\frac{\partial \underset{\sim}{\bar{S}}}{\partial t} = -\bar{\omega}\frac{\partial \underset{\sim}{\bar{S}}}{\partial p} + \frac{\underset{\sim}{E} - \underset{\sim}{\bar{S}}}{\tau} \qquad (22)$$

A time-scale $\tau \lesssim 1$ hr. will probably be satisfactory and prevent jolts to the thermodynamic structure when convection is initiated. Thus $(\underset{\sim}{S} - \underset{\sim}{E})$ will correspond to about 1 hour's forcing of the large-scale. Typically this will keep the atmosphere somewhat cooler and moister than $\underset{\sim}{E}$.

4.2.3 The component equations are (simplified)

$$\frac{\partial \bar{\theta}_E}{\partial t} = -\bar{\omega}\frac{\partial \bar{\theta}_E}{\partial p} + \frac{\theta_{EA} - \bar{\theta}_E}{\tau} \qquad (22a)$$

$$\frac{\partial \bar{\theta}}{\partial t} = -\bar{\omega}\frac{\partial \bar{\theta}}{\partial p} + \frac{\theta_A - \bar{\theta}}{\tau} \qquad (22b)$$

$$\frac{\partial \bar{q}}{\partial t} = -\bar{\omega}\frac{\partial \bar{q}}{\partial p} + \frac{q_A - \bar{q}}{\tau} \qquad (22c)$$

where the suffix A denotes the quasiequilibrium profile $\underset{\sim}{E}$. Initially the adjustment will move $\bar{\theta}$, $\bar{q}$ toward θ_A, q_A (which for example will typically cool the low levels). Then as quasiequilibrium is approached, the vector $\underset{\sim}{E} - \underset{\sim}{S}$ corresponds to a warming and drying by the convection. At low levels it will be a θ_E sink and at upper levels a θ_E source, because of the θ_E minimum in the profile of $\underset{\sim}{E}$.

4.2.4 The precipitation rate is

$$P = -\int \frac{(q_A - \bar{q})}{\tau}\frac{dp}{g} \qquad (23)$$

Initially the term $(q_A - \bar{q})$ may represent a moistening at some levels which correspondingly reduces P. It may be necessary to impose a constraint that $P \geqslant 0$ during the initial adjustment. (see 4.6.2, 4.7.1)

In quasiequilibrium $P = \int(\bar{\omega}\,\partial \bar{q}_A/\partial p)\,dp/g$ (24)

4.3 Equilibrium convective fluxes and structure

The relationship between these is an important aspect of the method. Near quasiequilibrium, $\underset{\sim}{S} \approx \underset{\sim}{E}$, for small τ and

$$\Delta \underset{\sim}{S} = (\underset{\sim}{E} - \underset{\sim}{S}) \approx \omega\tau(\partial \underset{\sim}{E}/\partial p) \qquad (25)$$

and the convective fluxes are given by

$$\underset{\sim}{F} = \left(\frac{\underset{\sim}{E} - \underset{\sim}{S}}{\tau}\right)\frac{dp}{g} = \int\frac{\Delta\underset{\sim}{S}}{\tau}\frac{dp}{g} \simeq \int\omega\left(\frac{\partial\underset{\sim}{E}}{\partial p}\right)\frac{dp}{g} \qquad (26)$$

The structure of the gradient of $\underset{\sim}{E}$ determines the structure of the fluxes near quasiequilibrium (if the vertical advection is the dominant large-scale forcing term). A vector difference $\Delta\underset{\sim}{S}$ has an associated BOWEN Ratio for the θ_L and total fluxes (Betts, 1983b). Level by level the convective flux divergence has the BOWEN Ratio of $\partial\underset{\sim}{E}/\partial p$. This is of importance: eg. the moist adiabat has a BR $\sim$-1, while the θ_{ESV} isopleth has B $\sim$ -0.8. If we specify a profile of $\underset{\sim}{E}$ corresponding to those observed (Section 3) then we impose in quasiequilibrium a corresponding convective heating and drying distribution (Q_1, Q_2 in the conventional notation): Fig. 22.

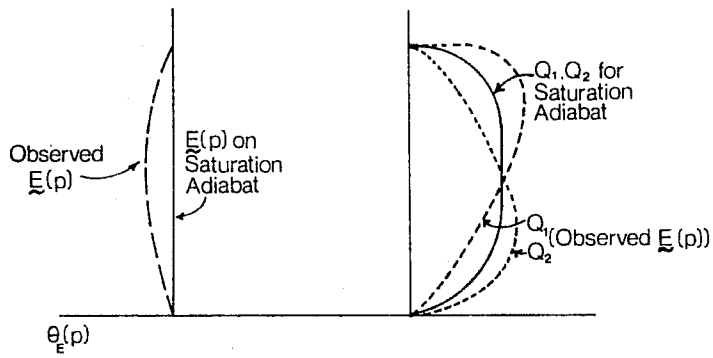

Fig. 22. Schematic θ_E structure and Q_1, Q_2 profiles for $\underset{\sim}{E}(p)$ saturated on moist adiabat (solid) and $\underset{\sim}{E}(p)$ to left of moist adiabat with near-constant $\mathcal{P}$.

Diagnostic budgets typically show $Q_2 > Q_1$ at low levels and a reversal above in agreement with this analysis. This is an upward advection of θ_E and represents a greater heating and reduced drying aloft in comparison with an adjustment which produces a moist adiabatic atmospheric structure. Of course, the maintenance of the more stable θ_{ES} structure aloft requires this. In this SP adjustment scheme therefore, both thermodynamic structure and fluxes in quasiequilibrium are directly coupled and have a realistic structure.

4.4 Initiation

I have not given this much thought yet. It is part of the general problem of transitions between boundary layer clouds and deep clouds. Following Kuo (1974), I would initiate deep convection in the presence of net moisture convergence, although here the convergence is not used to specify the convective amount.

SP adjustment needs a cloud-top to terminate the adjustment in the vertical. This may not be very critical. I propose defining cloud-top (h_T) at the intersection of the moist pseudo-adiabat through a low-level θ_E (before adjustment). Although the adjustment implicitly adjusts for buoyancy corrections due to liquid water loading and ice-phase processes, it seems unnecessarily complex to even

attempt to incorporate these in determining cloud-top. Ice/liquid water loading at cloud-top will be small and the ill-defined entrainment and freezing processes will at least partially cancel. I see no way of computing a realistic modified adiabat allowing for all the cloud thermodynamic processes, and there then remain the cloud dynamic processes which determine actual cloud-top.

4.5 θ_E constraint

A θ_E vertical structure will initially be specified, but this will then be shifted across the θ_E isopleths so that the convective adjustment satisfies a θ_E conservation constraint. Formally we require that the convection simply redistributes θ_E between the surface and cloud-top:

$$\int_{p_o}^{p_T} \frac{\theta_{EA} - \bar{\theta}_E}{\tau} dp = 0 \qquad (27)$$

This integral does not include the surface θ_E flux as this was included in the large-scale forcing (see 4.2.1) Unless precipitation falls as hail or snow at the surface, the correction for the freezing and melting processes is small in the integral.

4.6 Specification of $\underline{E}(p)$

This is a central part of the method, and it will need refinement beyond the proposal here.

4.6.1 First guess

Specify a $\theta_{ES}(p)$ structure starting at the surface wet-bulb temperature following a θ_{ESV} isopleth to the freezing level, and then a linear increase of θ_{ES} back to the surface value at 175 mb. Specify $\mathcal{P}(p)$ structure: I propose $\mathcal{P}$ = -30 mb as a suitable approximation (corresponding to a relative humidity ~85% at 800 mb and 75% at 500 mb). This gives the Saturation Level. From (θ_{ES}, p, p_{SL}) find $(\theta, q, \theta_E)^1_{SL}$.

4.6.2 θ_E constraint

Find mean θ_E correction $\delta\theta_E = \frac{1}{(p_o - p_T)} \int_{p_o}^{p_T} (\bar{\theta}_E - \theta_E^1) dp \qquad (28)$

and correct first guess at all levels. $\theta_{EA} = \theta_E^1 + \delta\theta_E \qquad (29)$

There are some options in correcting (θ, q) from this $\delta\theta_E$: see Fig. 23.

a) Preserve p_{SL} (and $\mathcal{P}$), thereby changing θ, q. I think this is desirable at low levels because the downdraft structure will tend to preserve a $\mathcal{P}$ structure as θ_E changes (Betts, 1982b).

b) Preserve θ, thereby changing q, $\mathcal{P}$. This will increase $|\mathcal{P}|$ to represent a lower RH if $\delta\theta_E$ is negative. This has possible advantages in delaying the moistening of the atmosphere. It might be necessary at high levels if the initial atmosphere is very dry, but if used at low levels would tend to uncouple the θ_E, θ_{ES} profiles which is undesirable ((b) will also give more precipitation then (a)).

Initially I suggest (a). The $\delta\theta_E$ correction to $\underset{\sim}{E}$ couples the entire troposphere θ_E adjustment. It might be desirable to uncouple the upper troposphere if it is initially very dry. Otherwise, the water vapor input needed to moisten it to give $\mathcal{P} \sim -30$ mb may reduce early precipitation too much. This needs modelling and observational study.

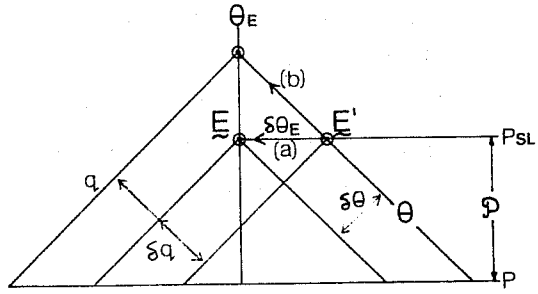

Fig. 23. Schematic showing relationship of $\delta\theta_E$ correction to $\delta\theta$, δq for cases (a), (b).

4.6.3 Time dependent $\mathcal{P}$ of equilibrium state $\underset{\sim}{E}$

Very dry initial atmospheres may take longer to adjust in the moisture field and this could be accomplished by allowing $\mathcal{P}$ to be time dependent (eg. -50 (decreasing) to -30). It is necessary to ensure $P \geqslant 0$ in Section 4.2.4.

Mesoscale complexes may tend to produce layer clouds on a longer time scale. This can be accomplished by allowing $\mathcal{P}$ to change toward, say +20 mb corresponding to a cloud-water field. We lack extensive statistics on mean layer cloud values of $\mathcal{P}$. Perhaps ISSCP will provide some information.

Whatever the time dependence of $\underset{\sim}{E}$, the procedure adjusts the convective fluxes, and the distribution of the moisture convergence into moistening (and liquid storage) and precipitation automatically. Initially some of the moisture convergence goes into moistening the mean atmosphere toward $\underset{\sim}{E}$ and then in quasi-equilibrium it is essentially all precipitated.

4.6.4 Dynamically different convective regimes

The equilibrium state $\underset{\sim}{E}$ may differ for dynamically different regimes. For example, fast-moving squall systems may reduce the boundary layer humidity further (to give $\mathcal{P} \sim -60$ mb), and give more extensive upper level cloud fields. To the extent we can relate this to grid-point variables, space dependent $\underset{\sim}{E}$ can be incorporated.

4.6.5 Subgrid-scale distributions of $\underset{\sim}{E}$

Fractional cloudiness at a grid point could be introduced with a distribution of $\mathcal{P}$ around a mean. The explicit modelling of the subgrid scale is needed. This may be necessary to describe the decay of layer clouds.

In the boundary layer the sharp contrast between inflow and outflow SP may not be well described by a single average, and may need a subgrid-scale specification. This may be true of all levels of strong outflow.

5. Conclusion

The intent is to provide a framework in which our observational understanding of convective equilibrium structure can be incorporated in numerical parameterizations of convection. Clearly much remains to be tested. If successful a model would always retain realistic vertical fluxes and thermodynamic structure in the presence of deep convection. I have addressed the problem of parameterizing deep convection, but the same approach can be used for a general boundary layer model. I have stated this elsewhere (see Section 2 and Betts 1983a). We need in fact a formulation which covers the entire span of convective regimes.

Acknowledgements

This work was supported by the National Science Foundation under grant ATM-8120444.

References

Barnes, G. M. and K. Sieckman, 1983: The Environment of Fast and Slow Tropical Mesoscale Convective Cloud Lines. Submitted to Mon. Wea. Rev.

Betts, A. K., 1976: Modelling Subcloud Layer Structure and Interaction with a Shallow Cumulus Layer. J. Atmos. Sci., 33, 2363-2382.

Betts, A. K. and M. F. Silva Dias, 1979: Unsaturated Downdraft Thermodynamics in Cumulonimbus. J. Atmos. Sci., 36, 1061-1071.

Betts, A. K., 1982a: Saturation Point Analysis of Moist Convective Overturning, J. Atmos. Sci., 39, 1484-1505.

Betts, A. K., 1982b: Cloud Thermodynamic Models in Saturation Point Coordinates, J. Atmos. Sci., 39, 2182-2191.

Betts, A. K., 1983a: Thermodynamics of Mixed Stratocumulus Layers: Saturation Point Budgets. J. Atmos. Sci. (Nov).

Betts, A. K., 1983b: Boundary Layer Thermodynamics of a High Plains Severe Storm (submitted to Mon. Wea. Rev.).

Deardorff, J. W., 1976: On the Entrainment Rate of a Stratocumulus Topped Mixed Layer. Quart. J. Roy. Meteor. Soc., 102, 563-582.

Deardorff, J. W., 1980a: Cloud-top Entrainment Instability. J. Atmos. Sci., 37, 131-147.

Frank, W. M., 1977: The Structure and energetics of the Tropical Cyclone Part I: Storm Structure. Mon. Wea. Rev., 105, 1119-1135.

Miller, M. J. and A. K. Betts, 1976: Travelling Convective Storms over Venezuela. Mon. Wea. Rev., 105, 833-848.

Randall, D. A., 1980: Conditional Instability of the First Kind Upside-down. J. Atmos. Sci., 37, 125-130.

Schubert, W. H., 1976: Experiments with Lilly's Cloud-topped Mixed Layer Model. J. Atmos. Sci., 33, 436-446.

Zipser, E. J. and M. A. Lemone, 1980: Cumulonimbus Vertical Velocity Events in GATE: Part II Synthesis and Model Core Structure. J. Atmos. Sci., 37, 2458-2469.